ACS NANO

www.acsnano.org

ARTICLE

Microscopic Detection Analysis of Single Molecules in MoS_2 Membrane Nanopores

Mingye Xiong, Michael Graf, Nagendra Athreya, Aleksandra Radenovic, and Jean-Pierre Leburton*

Cite This: *ACS Nano* 2020, 14, 16131–16139

Read Online

ACCESS | Metrics & More | Article Recommendations | Supporting Information

ABSTRACT: **A systematic microscopic analysis of the various resistive effects involved in the electronic detection of single biomolecules in a nanopore of a MoS_2 nanoribbon is presented. The variations of the transverse electronic current along the two-dimensional (2D) membrane due to the translocation of DNA and protein molecules through the pore are obtained by model calculations based on molecular dynamics (MD) and Boltzmann transport formalism, which achieved good agreement with the experimental data. Our analysis points to a self-consistent interaction among ions, charge carriers around the pore rim, and biomolecules. It provides a comprehensive understanding of the effects of the electrolyte concentration, pore size, nanoribbon geometry, and also the doping polarity of the nanoribbon on the electrical sensitivity of the nanopore in detecting biomolecules. These results can be utilized for fine-tuning the design parameters in the fabrication of highly sensitive 2D nanopore biosensors.**

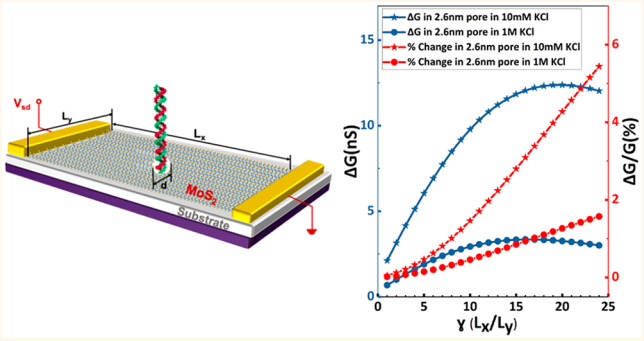

KEYWORDS: *2D materials, nanopores, biosensing, molecular dynamics, electron transport*

The use of nanopores in solid-state membranes has been proven to be compelling in the quest for the fast and accurate biomolecule sensing without labeling or functionalization by monitoring electronic signals.[1−6] Among all the materials of choice for nanoporous membranes, two-dimensional (2D) solid-state materials such as graphene and transition metal dichalcogenides (TMDs) stand out because of their sub-nanometer thickness comparable to the DNA base pair separation.

Standard experiments on DNA translocation through narrow nanopores have already demonstrated DNA or protein sensing by detecting the usual blockade of the ionic current flowing between two electrolytic cells separated by a 2D membrane.[7−9] Although early studies of graphene nanopores showed partial success,[10−13] they were impaired by the strong hydrophobic interaction between the membrane and nucleotides that results in severe sticking and clogging during DNA translocation.[14,15] In addition, they failed to expose the structural DNA details due to the low signal-to-noise ratio and the fast translocation speed. Alternatively, DNA translocation through the pore can be detected by the variations of the transverse electronic current flowing along a semiconducting TMD membranes such as molybdenum disulfide (MoS_2) that are less hydrophobic than graphene. Besides, long-term nanopore stability in TMD membranes has been demonstrated by us.[16,17] While still under experimental realization,[12] this approach has been predicted to result in larger and better resolved current signals with the potential for fast and reliable DNA sequencing.

Given the complexity of the nanopore systems involving the electric interaction between biomolecules, the ions in the electrolyte, and the 2D solid-state membranes, three different interpretations have been proposed to explain the origin of the transverse electronic current variations in the 2D membranes caused by the presence of DNA in the nanopore. They are (i) a capacitive effect between nanopore and solution,[18] (ii) a field-effect modulation of the carrier density in the membrane around the pore rim by the DNA charge screened by ions,[19] and (iii) the bare interaction between nucleotides and the nanopore with no ions in the scope.[20−22] Recently, a resistor circuit model was proposed to analyze the signal and noise of a 2D nanopore FET that excluded the latter interpretation (iii).[23] So far, no microscopic model has emerged to provide a coherent interpretation of the transverse current response to the DNA translocations in solid-state nanoribbon nanopores. In particular, the recent experimental observation of transverse

Received: October 6, 2020
Accepted: October 26, 2020
Published: November 6, 2020

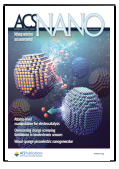

https://dx.doi.org/10.1021/acsnano.0c08382
ACS Nano 2020, 14, 16131−16139

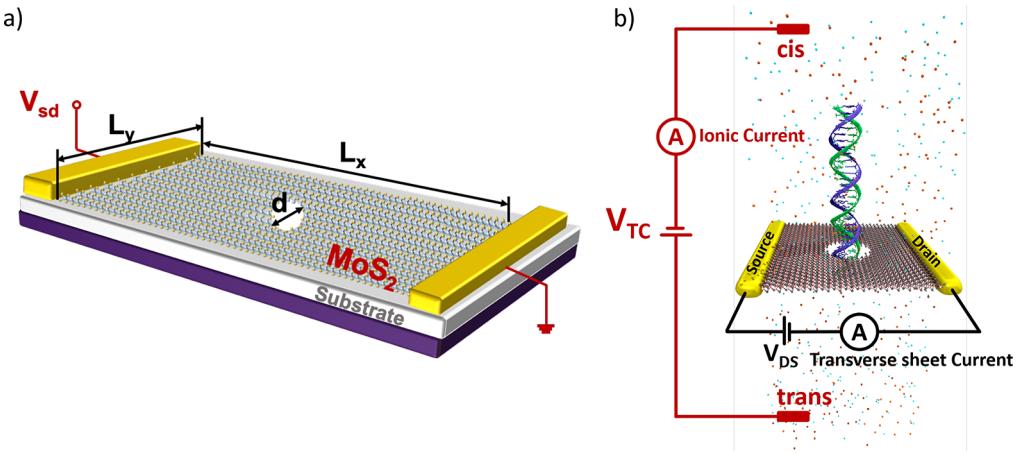

Figure 1. (a) Schematic (not to scale) of the MoS_2 membrane device for transverse current measurement. (b) Illustration of the system setup for dsDNA detection in electrolyte using both the ionic current measurement and transverse current.

current variations dependent on the charge sign of the translocating biomolecules[12] has not received a rigorous theoretical foundation.

In this work, we report on a comprehensive semiclassical analysis of the electronic current variation in a wide MoS_2 nanopore nanoribbon, which combines experimental transport characterization of the membrane with molecular dynamics and Poisson−Boltzmann modeling. The model takes into account the electrostatic potentials perturbing the charge carriers induced by the combined effect of the biomolecules, electrolyte, and ion screening around the pore rim, which produces variations in the transverse current signal across the membrane. Results obtained from our model are consistent with available experimental data. In this context, the model thus developed provides insight into the transverse conductance variations observed for a particular system configuration of the electrolyte concentration, pore size, and device geometry. In addition, it also provides guidelines to optimize the design parameters to fabricate a highly sensitive 2D nanopore biosensor.

The setup of a MoS_2 nanoribbon nanopore is illustrated in Figure 1a, where a semiconducting MoS_2 nanoribbon of width L_y and length L_x is lying on a substrate (usually SiN_x), with a pore of geometrical diameter d at the location (x_0, y_0). Two electrodes are placed at the two ends of the MoS_2 nanoribbon, between which a voltage V_{sd} is applied so that an electronic current flows along the nanoribbon (transverse current). In this setup, the presence of the nanopore in the semiconducting nanoribbon acts as a scattering center for the electronic flow. Moreover, salt ions and DNA molecules passing through induce a time-varying electrostatic potential at the rim of the nanopore membrane, which modulates the strength of the scattering center, thereby causing transverse current variations. Thus, by virtue of its sensitivity to the electrostatic properties of the nanopore, the scattered current ultimately detects the details of the DNA translocation.

In order to investigate the influence of the scattering nanopore on the MoS_2 conducting electrons, we treat the electrostatic potential variations as a perturbation to the transverse current and use Fermi's golden rule to assess its effect on the electronic conductivity. As the nanopore is 2−5 nm wide, which is much smaller than the width of the MoS_2 membrane ($L_y \sim 100-200$ nm), one can model the perturbative nanopore as Dirac delta function potential

$$V(\vec{r}) = V_{tot}\delta(x - x_0)\,\delta(y - y_0)A_{np} \tag{1}$$

where (x_0, y_0) is the position of the nanopore center, A_{np} is the area of the nanopore, and V_{tot} is the strength of the perturbation energy that consists in the combined electrostatic effects of DNA, ions, and nanopore onto the conducting electrons. Because of the narrow width of the 2D MoS_2 membrane, we assume that conducting electrons are charge carriers confined in the y-direction, moving freely along the x-direction of the nanoribbon. Charge carriers are represented by their quantum mechanical wave function $\psi = Ce^{ikx}\sin\left(\frac{n\pi y}{L_y}\right)$ with the kinetic energy $E_{k,n,\alpha} = \frac{\hbar^2k^2}{2m_\alpha} + E_n$, where k is the electron wave vector in the x-direction, $E_n = \frac{\hbar^2n^2\pi^2}{2m_\alpha L_y^2}$ is the nth ($n = 1, 2, ...$) sub-band energy in the y-direction, and m_α is the effective mass of the electrons in the valley α in the MoS_2 band structure. Here, $C = \sqrt{\frac{2}{L_xL_y}}$ is the normalization constant of the wave function. Thus, from Fermi's golden rule, the scattering rate of a single scattering from the (n, k) state to (n', k') is

$$S(\alpha, k, k', n, n') = \frac{8\pi V_{tot}^{\,2}A_{np}^{\,2}}{\hbar L_x^{\,2}L_y^{\,2}}\sin^2\left(\frac{n\pi y_0}{L_y}\right)\sin^2\left(\frac{n'\pi y_0}{L_y}\right)\delta(E_{k',n',\alpha} - E_{k,n,\alpha}) \tag{2}$$

where L_x is the length of the MoS_2 nanoribbon.

By summing over all initial (n, k) and final (n', k') states and using the linear response of the Boltzmann transport equation, we obtained the contribution to the membrane conductance solely caused by electron scattering by the nanopore delta potential

$$G_{pore} = \frac{F}{V_{tot}^{\,2}A_{np}^{\,2}} \tag{3}$$

where F is the form factor:

https://dx.doi.org/10.1021/acsnano.0c08382
ACS Nano 2020, 14, 16131−16139

$$F_\alpha(L_y, y_0, E_f^\alpha) = -\frac{e^2}{2\pi}\frac{\hbar^2 {L_y}^2}{2\sqrt{2m_\alpha}^3}\sum_n \sin^{-2}\left(\frac{n\pi y_0}{L_y}\right)\int \frac{\sqrt{E-E_n}\,dE}{\sum_{n'}\frac{\sin^2\left(\frac{n'\pi y_0}{L_y}\right)}{k'(k,n,n')}}\frac{\partial f_\alpha(E)}{\partial E} \quad (4)$$

Here, $f_\alpha(E)$ is the Fermi function of electrons in the MoS_2 valley α with the Fermi level E_f^α calculated with respect to the energy minimum of the valley. This form factor encapsulates the details of the nanoribbon geometry, pore position, material properties (such as carrier effective mass), and the carrier concentration. MoS_2 has been reported to consist of two valley minima in the conduction band corresponding to the K and Q valleys with slight energy difference $\Delta E_{QK} \approx 70$ meV and different effective mass $m_K = 0.5m_0$ and $m_Q = 0.78m_0$, so the overall form factor is $F(L_y, y_0) = F_K(L_y, y_0, E_f^K) + F_Q(L_y, y_0, E_f^Q)$. In Figure 2, we display the form factor for different pore positions and various carrier concentrations, which shows significant variations with the pore position.

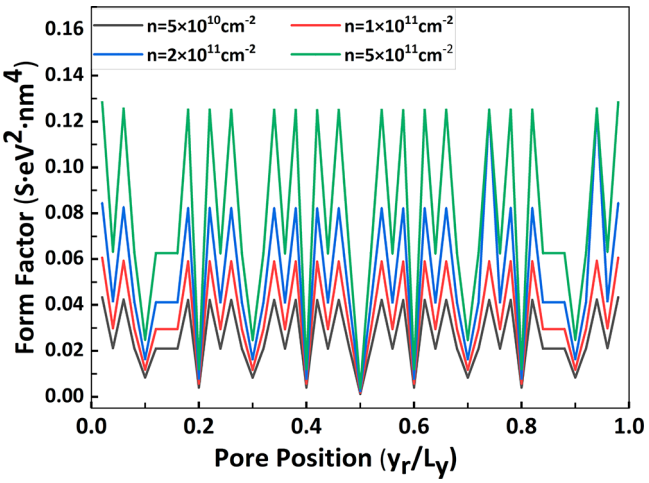

Figure 2. Form factor of the MoS_2 nanoribbon as calculated for various carrier concentrations and as a function of the pore position.

The high sensitivity of the form factor to pore position roots in the confinement of the charge carriers in the y-direction. When the pore is coincided with the nodes of the sinusoidal waves, the electrons in the nanoribbon will sense little variation due to the existence of the pore and thus result in a small form factor (see practical discussion in the Supporting Information, Section S5, "Comment on Form Factor"; and Section S6, "Comment on Experimental Precision of Pore Drilling"). Taken into account intrinsic nanopore scattering mechanisms, the total nanoribbon conductance is given by Matthiessen's rule[24]

$$\frac{1}{G_{tot}} = \frac{1}{G_{ribbon}} + \frac{\gamma}{G_{pore}} \quad (5)$$

where $\gamma = L_x/L_y$ is the nanoribbon geometry aspect ratio, and G_{ribbon} is the MoS_2 nanoribbon conductance in the absence of nanopore.

As mentioned above, the total perturbation potential V_{tot} causing the variations of the electronic transverse current compared to those of a bare MoS_2 nanoribbon consists of all three effects

$$V_{tot} = V_{pore} + V_{electrolyte} + V_{DNA} \quad (6)$$

These effects are the perturbation due to the pore alone V_{pore}, the perturbation due to the presence of the electrolyte ions in the pore $V_{electrolyte}$, and that of the DNA in the pore V_{DNA}. In open pore, only the nanopore and electrolyte contribute to the total perturbation energy, $V_{tot}^{open} = V_{pore} + V_{electrolyte}^{open}$. Ideally, aside from the noise due to the ion stochastic transport, this perturbation remains unchanged throughout time (see the discussion on noise behavior in the Supporting Information, Section S7). The transverse current due to these two factors sets the base current of a DNA translocation measurement. As a DNA molecule translocates through the nanopore, in addition to the DNA perturbation potential V_{DNA} induced to the nanopore rim, both ions and counterions in the electrolyte rearrange in the pore due to the DNA charge, thereby resulting in a change in the electrolyte perturbation $\Delta V_{electrolyte}$. Both the DNA presence and the redistribution of ions in the pore constitute the source of the transverse sensing signal.

In order to identify the contribution of each component of the total nanopore potential to the overall conductance variations, we measured the conductance of the pristine nanoribbon and open pore nanoribbon experimentally to obtain V_{tot}^{open}. Subsequently, we performed molecular dynamics (MD) simulation to obtain the trajectory of the potential variation on the pore rim through the translocation of a biomolecule in the MoS_2 nanopore biosensor with variant geometry and electrolyte concentration parameters. As shown in Figure 1b, the nanopore nanoribbon separates two electrolytic chambers. One pair of vertical electrodes is applied driving the DNA translocation as well as generate the ionic current. One pair of lateral electrodes is attached to the nanoribbon to drive and measure the transverse current along the nanoribbon.

First, we focus on the transverse electronic conductance resulting from the presence of an open pore to extract the potential $V_{pore} + V_{electrolyte}$. For this purpose, we experimentally measure the conductance of a MoS_2 nanoribbon in vacuum and the conductance of the same nanoribbon after drilling the nanopore in the presence of 1 M KCl solution (see the method section in Graf *et al.*[12] for the experiment and material details.) The MoS_2 nanoribbon is $L_y = 500$ nm wide and $L_x = 2$ μm long. The nanopore with a diameter $d = 5.2$ nm is located at the center of the nanoribbon at $y_0/L_y = 0.5$. We obtain the bare MoS_2 nanoribbon $G_{ribbon} = 1.96$ μS, and $G_{tot}^{op} = 1.1$ μS for the open pore measurement, as shown in Figure 3, yielding $G_{pore} = 10$ μS for $\gamma = \frac{L_x}{L_y} = 4$.

Recent experimental and theoretical works[25−30] have shown that electrons in a single layer MoS_2 are characterized by a mobility ranging from 10 to 50 $cm^2\ V^{-1}\ s^{-1}$, from which, based on the nanoribbon conductance, the carrier concentration varies between 0.61×10^{11} and 3.1×10^{11} cm^{-2} corresponding to a Fermi level between 67 and 46 meV below the conduction band edge. Based on these values, one can calculate the form factor ranging between $F = 1.40 \times 10^{-3}$ and $F = 3.04 \times 10^{-3}$ S eV^2 nm^4. By combining eqs 3 and 5 into

$$V_{tot} = \sqrt{\left(\frac{1}{G_{tot}} - \frac{1}{G_{ribbon}}\right)\frac{F}{\gamma}\frac{1}{A_{np}^2}} \quad (7)$$

one can estimate the open pore potential V_{tot}^{open} to vary between 0.56 and 0.82 eV. In this way, the pore potential obtained

https://dx.doi.org/10.1021/acsnano.0c08382
ACS Nano 2020, 14, 16131−16139

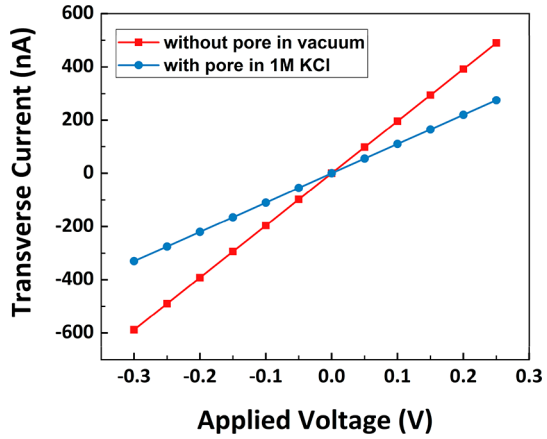

Figure 3. $I-V$ curves of the MoS_2 nanoribbon in vacuum before drilling the pore (red curve) and after pore drilling (blue curve) in the center of the nanoribbon in a 1 M KCl solution with pore diameter equal to 5.9 nm.

describes not only the existence of the nanopore but also the degradation or additional effect that can possibly inflict on the membrane conductance. The effect of the electron beam in the pore drilling process is irreversible, which suggests physical damage to the layer. Most probably, sulfur vacancies are responsible for the reduction in the mobility.[31,32] The degradation also contributes to the decrease in conductance. This degradation effect is also included in the V_{pore} potential.

RESULTS AND DISCUSSION

In this study, we performed all-atom MD to simulate the electrophoresis of biomolecules in the MoS_2 nanopore of diameter 2.6 and 5.2 nm in high and low electrolyte concentration for comparison. The list of all MD simulations and the corresponding relevant details are provided in the Supporting Information, Section S1. We extract the DNA charge distributions during the translocation. We then use a self-consistent Poisson−Boltzmann scheme to calculate the

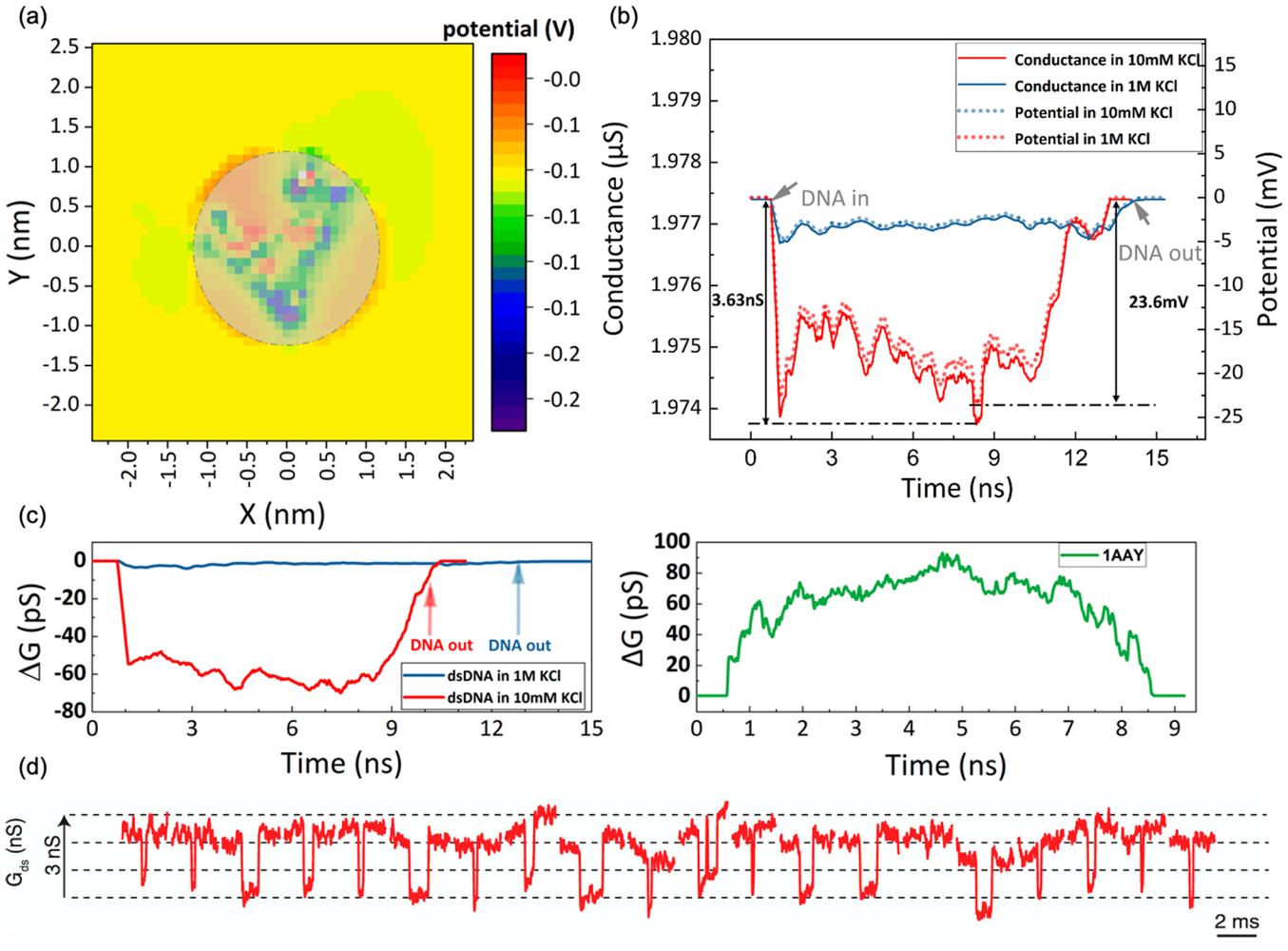

Figure 4. (a) Potential color plot in the pore and around the pore rim for a dsDNA translocation through a 2.6 nm pore in a MoS_2 membrane at t = 4 ns in a 10 mM KCl solution. The gray shaded area represents the pore. The potential outside the pore is compiled for the calculation of electron scattering. (b) Potential and transverse conductance variation during a 30 bp dsDNA translocation through a 2.6 nm MoS_2 nanopore in uniform 10 mM KCl and 1 M KCl solutions: the conductance in 10 mM KCl shows a clear signal of translocation which agrees well with the experimental results displayed in part d below. (c) Transverse conductance variation during the biomolecule translocation through the 5.2 nm MoS_2 nanoribbon nanopore. Left: 30 bp dsDNA translocation in 10 mM KCL and 1 M KCl; Right: translocation of a positively charged protein 1AAY in 10 mM KCl. (d) Experimental traces of multiple 1 kb dsDNA translocating through a 2.5 nm pore in a 10 mM to 1 M (cis−trans) KCl solution. The magnitude of the dips is in agreement with the theoretical results displayed in part b. Part d is reprinted with permission from ref 12. Copyright 2019 American Chemical Society.

https://dx.doi.org/10.1021/acsnano.0c08382
ACS Nano 2020, 14, 16131−16139

electrical potential variations arising from the redistribution of ion charges caused by the presence of DNA in the nanopore. The details of MD simulation and self-consistent Poisson–Boltzmann scheme are described in the Methods section.

In Figure 4a, we display the color map of the electric potential that exhibits significant negative values due to the negative charge of the DNA backbones inside a nanopore of 2.6 nm diameter in 1 M KCl electrolyte. From the color code, one can clearly see that the negative potential extends inside the MoS_2 membrane, which adds to the electron scattering by the pore and the ions and in turn modifies the transverse electronic current. After compiling the values of the DNA potential variations around the pore for each time frame of the DNA trajectory obtained by MD, one obtains the potential variation of the DNA translocation event as a function of time.

Figure 4b (right scale) compares the traces of the potential variations around a 2.6 nm wide nanopore for 30 bp dsDNA translocation in uniform 10 mM KCl and 1 M KCl solution, where it is seen that both the potential change and the translocation time differ between the translocations in different molarities. The dwell time of 30 bp dsDNA translocation through 2.6 nm pore in 1 M KCl solution is observed to be 12.57 ns, which is nearly 2 ns slower than its counterpart in 10 mM KCl solution (10.62 ns). This time difference in translocation is also observed in the 5.2 nm pore as shown in Figure 4c, left. The tardiness of translocation in a higher-concentration electrolyte solution is due to the increased resistance by the ions toward the translocating molecule, which has been observed before in 3D solid-state nanopores such as glass[33] and Si_3N_4 nanopores.[34]

The potential variations arising from DNA translocation in a 10 mM KCl solution result in a ∼20 mV amplitude change on the pore rim, while in a 1 M KCl solution, the potential variation amplitude is smaller and reaches barely ∼6 mV at its maximum value. We now proceed to calculate the transverse current by using our transport model eqs 5 and 6. As shown in Figure 4b (left scale), the transverse conductance for a dsDNA translocation event in 10 mM KCl varies with an amplitude of ∼4 nS. As a consequence of the reduced potential variations in high electrolytic concentration, the conductance variations in 1 M KCl are below 1 nS, which is too small to be observed experimentally.

This amplitude difference of potential and conductance change between DNA translocation in 10 mM and 1 M KCl is due to the ion screening effect characterized by the Debye length, which in water at room temperature is $\lambda_d = \frac{0.304}{\sqrt{I(M)}}$ (in nm), where I is the ionic molar concentration (M). Hence, in 10 mM KCl solution, $\lambda_d \sim 3$ nm, whereas in 1 M KCl solution, it is 1/10 that length, *i.e.*, ∼0.3 nm. This larger electrical sensitivity of MoS_2 nanopores in lower electrolytic concentration is in qualitative agreement with recent experimental data. Thus, MoS_2 in a lower-concentration electrolyte can sense more of the potential change coming from DNA translocation. The simulations also show that the fluctuations of the potential variations (in the order of a few mV for the 10 mM KCl electrolyte) are caused by mainly the stochastic DNA conformational variations during the translocation event and the redistribution of ions due to the DNA charge in the pore $\Delta V_{electrolyte}$.

In a gradient concentration system, which is usually employed in solid-state nanopore experiments to slow down the biomolecule translocation, one can use our model with a uniform KCl concentration of the lower molarity to reach a good approximation to the actual conductance change. Subsequently, in order to obtain a more precise transverse conductance change, one can interpolate between the two transverse conductance changes obtained from uniform concentration systems corresponding to the two molarities used for the gradient concentration. This agrees well in the order of magnitude with the experimental results as shown in Figure 4d.[12]

These electric variation effects are relatively small compared to the presence of the pore itself and the ions in the open pore, *i.e.*

$$V_{DNA} + \Delta V_{electrolyte} = \delta V \ll V_{tot}^{open} = V_{pore} + V_{electrolyte}^{open}$$

This results in a relatively small conductance change δG in the MoS_2 ribbon, so that

$$\frac{1}{G_{tot}^{op} + \delta G} = \frac{1}{G_{ribbon}} + \frac{\gamma (V_{tot}^{open} + \delta V)^2 {A_{np}}^2}{F} \tag{8}$$

where

$$\frac{1}{G_{tot}^{op}} = \frac{1}{G_{ribbon}} + \frac{\gamma (V_{tot}^{open})^2 {A_{np}}^2}{F} \tag{9}$$

From eqs 8 and 9, one obtains the linear relation between δG and δV, *i.e.*

$$\delta G = -\frac{2\gamma {A_{np}}^2 V_{tot}^{open} G_{tot}^{op^2}}{F} \delta V \tag{10}$$

From eq 10, conductance variation is inversely proportional to the form factor. Referring to Figure 2, it is seen that placing the nanopore at the center of the ribbon gives the highest conductance for the most sensitive biodetection. However, other positions at $y_0 = \frac{1}{5}L_y, \frac{2}{5}L_y, \frac{3}{5}L_y, \frac{4}{5}L_y$ are favorable as well. Furthermore, higher carrier concentration gives higher sensitivity.

Also, in eq 10, one notices that when V_{tot}^{open} and δV are of the same sign, the conductance correction due to DNA translocation in the nanopore is negative as shown in Figure 4b. Here, the negative charges on the DNA backbones induce a negative electric potential on the nanopore rim, which increases the electron perturbation energy in the MoS_2 nanoribbon, thereby decreasing the electronic conductance. This sign dependence of the perturbation energy on the charge of the translocating biomolecule is consistent with recent experiments that show an increase of the transverse conductance during translocation of positively charged polylysine protein.[12] For this reason, we further performed the same kind of simulation of a translocating positively charged 1AAY protein, for which, owing to the protein size, we enlarge the pore to 5.2 nm diameter. Figure 4b displays the transverse conductance variations for both translocating biomolecules, *i.e.*, 1AAY protein and DNA, showing opposite variations with the former conductance increasing and the latter decreasing, as expected. In this comparison, it should be emphasized that, in the case of *p*-type MoS_2, *i.e.*, the charge carriers are holes, V_{tot}^{open} will be inverted and the conductance variations will also be inverted for both types of biomolecules, so that the sign of the conductance variation is not only due to the charge of the biomolecule, DNA, or proteins, which

https://dx.doi.org/10.1021/acsnano.0c08382
ACS Nano 2020, 14, 16131−16139

determines the sign of δV, but also due to the membrane type, as well as the nanopore charge that determines V_{tot}^{open}.

As the electronic conductance variation δG captures the features of the DNA translocation signal, by amplifying its value one enhances the sensitivity of the MoS_2 nanopore biosensor. Among the different factors shaping δG, the nanoribbon geometry depicted by the geometric aspect ratio $\gamma = L_x/L_y$ is critical. As shown in eq 10, δG is proportional to γ and inversely proportional to F, and thereby inversely proportional to L_y. In Figure 5 (top), we display the absolute

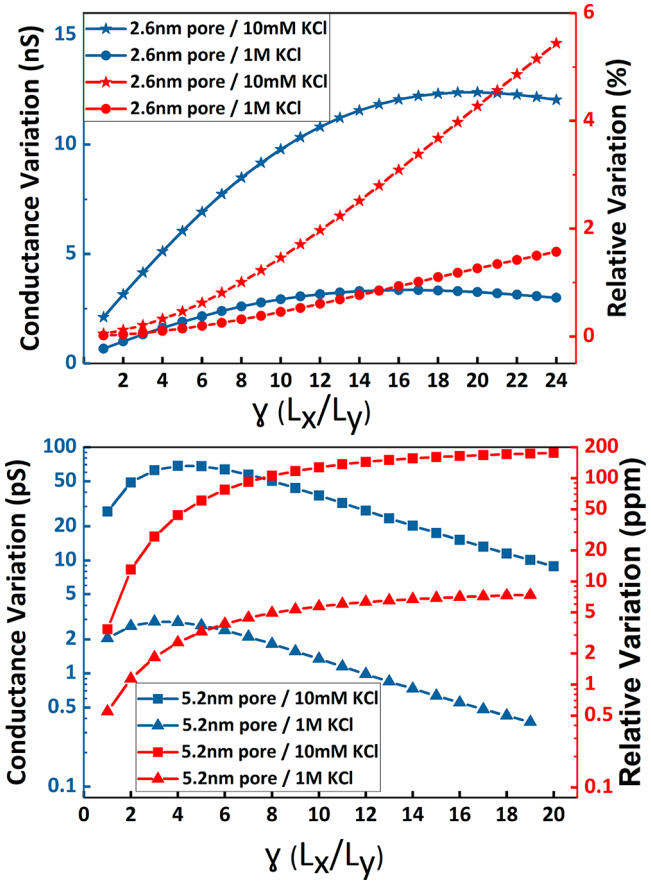

Figure 5. Absolute and relative conductance variation of a dsDNA translocation event through a 2.6 nm pore (top) and 5.2 nm pore (bottom) as a function of the MoS_2 nanoribbon geometric aspect ratio ($\gamma = L_x/L_y$).

and relative conductance variation δG (left scale) and $\delta G/G$ (right scale), respectively, as a function of γ, where one can see that δG exhibits a maximum at $\gamma = 16$ for 1 M KCl and at $\gamma = 20$ for 10 mM KCl. This behavior is the consequence of the decreasing dependence of the open-pore conductance G_{tot}^{op} on γ, as clearly seen in the monotonic variation of $\delta G/G$ with the geometric aspect ratio. The phenomenon dominates with the 5.2 nm pore, as shown in Figure 5 (bottom) that displays the maximum of $\delta G \approx 2.9$ pS at $\gamma = 3$ in 1 M KCl and $\delta G \approx 68$ pS at $\gamma = 4$ in 10 mM KCl and decreases drastically as γ further increases (the width L_y further shrinks).

Another key factor that affects the sensitivity is the pore size, which can be seen by comparing the conductance signal in a 2 nm (Figure 4a) and a 5.2 nm pore (Figure 4b), where one observes a sensitivity difference of about 60 times larger in the former. This large difference results from the fact that a wider pore experiences reduced DNA perturbation variations caused by the screening of the ions determined by the Debye length, λ_d. However, in eq 10, one also sees that as the pore size (A_{np}) increases, the conductance variation induced by the biomolecule translocation increases. For the two simulated nanopore sizes, one observes that the decrease in δV plays a more significant role, and thus a smaller nanopore gives a higher sensitivity. In general, however, sensitivity optimization is a delicate balance between the two factors A_{np} and δV for molecules with specific size.

CONCLUSIONS

In this paper, we use a combined experimental–theoretical approach to analyze in detail the biosensing process in a nanopore by transverse electronic current variations in a MoS_2 membrane nanoribbon. Our microscopic analysis offers a direct connection between the transverse current response to biomolecule translocations in the nanopore and the different components of the electrical resistance of the membrane, *i.e.*, electrolyte, open pore, and DNA motion. In particular, our model based on the Boltzmann transport formalism emphasizes not only the effects of the electrolyte concentration, pore size, and the nanoribbon geometric aspect ratio $\gamma = L_x/L_y$ but also that of the doping polarity of the nanoribbon, on the electrical sensitivity of the nanopore. These effects underline the microscopic interaction among the three charged systems at play in the detection mechanism, *i.e.*, ions, biomolecules, and charge carriers in the membrane. As a result, we note that the transverse electronic conductance response to dsDNA translocation in a 2.6 nm pore agrees well with experimental results. Finally, let us point out that our model for nanopore biosensing can easily be extended to any 2D material other than MoS_2 by accounting for the details of the material electronic band structure.

METHODS

Molecular Dynamics (MD) Simulations. In the first step of the simulations, the intended nanopore system was built using all-atom molecular dynamics (MD) software complemented by the Visual Molecular Dynamics (VMD) software for system analysis,[35] while 9 nm × 9 nm MoS_2 membranes were constructed in the VMD. Lennard-Jones (LJ) parameters from Stewart *et al.*[36] were incorporated for the atoms in the MoS_2 monolayer, and all the atoms in the MoS_2 membrane were fixed to their initial positions to avoid the drifting of the membrane during the simulations. The translocation behavior of the DNA through MoS_2 nanopore, especially the biomolecule's conformational fluctuations, is dominated by the nonbonded interactions between the DNA and the atoms in MoS_2. Hence, our choice of fixed MoS_2 membrane with only LJ parameters defined for interactions seems to be valid in this scenario. Then, nanopores in the membrane were created by manually removing relevant atoms. The Mo and S atoms of the MoS_2 membrane at the pore edges are considered to have no partial charge after the creation of the nanopore.

The dsDNA structure comprising a random sequence was obtained from the 3D-DART web server[37] and was described using CHARMM27 force fields.[38] For illustrating the device performance on the positively charged molecule, Zif268 protein–DNA complex (PDB code: 1AAY), a DNA binding protein which is inherently positively charged (11e), was considered.[39] The protein was described using the CHARMM22 force field with CMAP corrections. To shorten the simulation time, the DNA molecule or protein was placed above the nanopore to begin the translocation. The whole system is solvated in a water box, and ions (potassium and chlorine) are randomly placed in the box to reach a concentration of 10 mM or 1

https://dx.doi.org/10.1021/acsnano.0c08382
ACS Nano 2020, 14, 16131–16139

M. The water molecules and ions were defined by the TIP3P model[40] and CHARMM27 with NBFIX corrections,[41] respectively. For dsDNA translocation studies, an electric field of 1 V is applied perpendicular to the nanopore membrane to drive the dsDNA through the pore. However, for the protein translocation case study, the biomolecule was translocated artificially through the MoS_2 nanopore in the absence of all-atom MD simulations as previously performed by Girdhar *et al.*[42] Due to the utilization of this method, we do not observe any folding/unfolding of the 1AAY protein in the pore. A more detailed description of the simulated systems is provided in the Supporting Information, Table S1.

The MD simulations are performed using NAMD 2.13.[43] The systems are maintained at 300 K using a Langevin thermostat. Periodic boundary conditions are employed in all directions. Time steps of 2 fs along with a particle Mesh Ewald[44] were used to treat long-range electrostatics. All systems are minimized for 5000 steps, followed by a 600 ps equilibration as an NPT ensemble. The systems are further equilibrated as an NVT ensemble for another 2 ns before the electric field is applied. The trajectories of all atoms in the system are recorded at every 5000 steps until the DNA is completely translocated.

Our previous works of dsDNA translocations through MoS_2 nanopore membranes[45,46] and three simulations performed with different initial conditions (for dsDNA translocating through 2.6 nm pore in 1 M KCl solution) suggest that the only change in the simulations observed were that of the conformational fluctuations of the DNA while translocating through the pore. These conformational fluctuations of the DNA would only change the variations in the conductance trace obtained along the MoS_2 while the DNA is translocating. However, this does not change the relative magnitude of the open-pore conductance to the blocked-pore conductance. Hence, we believe that the proposed methodology for analyzing single-molecule transport in MoS_2 nanopore FETs remains valid for any system initialized with random initial conditions.

Potential Calculations. For each frame in the MD trajectory, electrostatic potential, $\varphi(r)$, is calculated using Poisson–Boltzmann's equation shown in eq 11.

$$\nabla\cdot[\epsilon(r)\nabla\varphi(r)] = -e[C_{K^+}(r) - C_{Cl^-}(r)] - \rho_{DNA/protein}(r) - \rho_{semiconductor}(r) \tag{11}$$

where $\rho_{DNA/protein}(r)$ is the charge due to DNA or protein, $\rho_{semiconductor}(r)$ the mobile charges in the MoS_2 layer, and $\epsilon(r)$ the local permittivity, and $C_{K^+}(r)$ and $C_{Cl^-}(r)$ are the local electrolyte concentrations of K^+ and Cl^- that obey Poisson–Boltzmann statistics given by the following equations.

$$C_{K^+}(r) = C_0 \exp\left[\frac{-e\varphi(r)}{k_B T}\right] \tag{12}$$

$$C_{Cl^-}(r) = C_0 \exp\left[\frac{e\varphi(r)}{k_B T}\right] \tag{13}$$

Here, C_0 is the nominal concentration in the solution, which is set to 10 mM or 1 M. The above two equations are solved numerically until the convergence criterion is met. A detailed description of charge distributions is given by Girdhar *et al.*[42]

ASSOCIATED CONTENT

Supporting Information

The Supporting Information is available free of charge at https://pubs.acs.org/doi/10.1021/acsnano.0c08382.

Molecular dynamics simulation list; ionic signal as a function of time during DNA translocations; notes on molecular dynamics simulation; additional information on transverse conductance trace; comments on form factor; comments on experimental precision of pore drilling; and comments on noise behavior (PDF)

AUTHOR INFORMATION

Corresponding Author

Jean-Pierre Leburton − *Department of Electrical and Computer Engineering, and N. Holonyak Jr. Micro & Nanotechnology Laboratory, University of Illinois at Urbana−Champaign, Urbana, Illinois 61801, United States;* orcid.org/0000-0002-8183-5581; Email: jleburto@illinois.edu

Authors

Mingye Xiong − *Department of Electrical and Computer Engineering, and N. Holonyak Jr. Micro & Nanotechnology Laboratory, University of Illinois at Urbana−Champaign, Urbana, Illinois 61801, United States;* orcid.org/0000-0003-0826-4118

Michael Graf − *Laboratory of Nanoscale Biology, Institute of Bioengineering, School of Engineering, Ecole Polytechnique Federale de Lausanne, Lausanne CH 1015, Switzerland;* orcid.org/0000-0001-6201-7471

Nagendra Athreya − *Department of Electrical and Computer Engineering, and N. Holonyak Jr. Micro & Nanotechnology Laboratory, University of Illinois at Urbana−Champaign, Urbana, Illinois 61801, United States*

Aleksandra Radenovic − *Laboratory of Nanoscale Biology, Institute of Bioengineering, School of Engineering, Ecole Polytechnique Federale de Lausanne, Lausanne CH 1015, Switzerland;* orcid.org/0000-0001-8194-2785

Complete contact information is available at: https://pubs.acs.org/10.1021/acsnano.0c08382

Author Contributions

M.X. derived the analytical model and data analysis under J.-P.L.'s supervision. N.A. performed the MD simulations. M.G. and A.R. provided insightful data and supported the work through discussions that detail the real-world conditions of the experiment. All authors provided constructive comments on the manuscript.

Notes

The authors declare no competing financial interest.
A preprint version of this work is available on arXiv.[47]

ACKNOWLEDGMENTS

M.X., N.A., and J.-P.L. are indebted to Oxford Nanopore Technology and the Illinois Proof-of-Concept (i-POC) program for supporting this study and gratefully acknowledge supercomputer time provided through the Extreme Science and Engineering Discovery Environment (XSEDE) Grant TG-MCB170052. M.G. and A.R. acknowledge support from the Swiss National Science Foundation (SNSF) Consolidator grant (BIONIC BSCGI0_157802) and CCMX project ("Large Area Growth of 2D Materials for Device Integration").

REFERENCES

(1) Dekker, C. Solid-State Nanopores. *Nat. Nanotechnol.* **2007**, *2* (4), 209–215.
(2) Gracheva, M. E.; Aksimentiev, A.; Leburton, J.-P. Electrical Signatures of Single-Stranded DNA with Single Base Mutations in a Nanopore Capacitor. *Nanotechnology* **2006**, *17* (13), 3160–3165.
(3) Gracheva, M. E.; Vidal, J.; Leburton, J.-P. P - n Semiconductor Membrane for Electrically Tunable Ion Current Rectification and Filtering. *Nano Lett.* **2007**, *7* (6), 1717–1722.

(4) Yusko, E. C.; Bruhn, B. R.; Eggenberger, O. M.; Houghtaling, J.; Rollings, R. C.; Walsh, N. C.; Nandivada, S.; Pindrus, M.; Hall, A. R.; Sept, D.; Li, J.; Kalonia, D. S.; Mayer, M. Real-Time Shape Approximation and Fingerprinting of Single Proteins Using a Nanopore. *Nat. Nanotechnol.* **2017**, *12* (4), 360−367.
(5) Siwy, Z.; Fuliński, A. Fabrication of a Synthetic Nanopore Ion Pump. *Phys. Rev. Lett.* **2002**, *89* (19), 198103.
(6) Niedzwiecki, D. J.; Grazul, J.; Movileanu, L. Single-Molecule Observation of Protein Adsorption onto an Inorganic Surface. *J. Am. Chem. Soc.* **2010**, *132* (31), 10816−10822.
(7) Garaj, S.; Hubbard, W.; Reina, A.; Kong, J.; Branton, D.; Golovchenko, J. A. Graphene as a Subnanometre Trans-Electrode Membrane. *Nature* **2010**, *467* (7312), 190−193.
(8) Feng, J.; Liu, K.; Bulushev, R. D.; Khlybov, S.; Dumcenco, D.; Kis, A.; Radenovic, A. Identification of Single Nucleotides in MoS2 Nanopores. *Nat. Nanotechnol.* **2015**, *10* (12), 1070−1076.
(9) Nicolaï, A.; Barrios Pérez, M. D.; Delarue, P.; Meunier, V.; Drndić, M.; Senet, P. Molecular Dynamics Investigation of Polylysine Peptide Translocation through MoS 2 Nanopores. *J. Phys. Chem. B* **2019**, *123* (10), 2342−2353.
(10) Schneider, G. F.; Kowalczyk, S. W.; Calado, V. E.; Pandraud, G.; Zandbergen, H. W.; Vandersypen, L. M. K.; Dekker, C. DNA Translocation through Graphene Nanopores. *Nano Lett.* **2010**, *10* (8), 3163−3167.
(11) Merchant, C. A.; Healy, K.; Wanunu, M.; Ray, V.; Peterman, N.; Bartel, J.; Fischbein, M. D.; Venta, K.; Luo, Z.; Johnson, A. T. C.; Drndić, M. DNA Translocation through Graphene Nanopores. *Nano Lett.* **2010**, *10* (8), 2915−2921.
(12) Graf, M.; Lihter, M.; Altus, D.; Marion, S.; Radenovic, A. Transverse Detection of DNA Using a MoS 2 Nanopore. *Nano Lett.* **2019**, *19* (12), 9075−9083.
(13) Sathe, C.; Zou, X.; Leburton, J.-P.; Schulten, K. Computational Investigation of DNA Detection Using Graphene Nanopores. *ACS Nano* **2011**, *5* (11), 8842−8851.
(14) Wells, D. B.; Belkin, M.; Comer, J.; Aksimentiev, A. Assessing Graphene Nanopores for Sequencing DNA. *Nano Lett.* **2012**, *12* (8), 4117−4123.
(15) Lv, W.; Chen, M.; Wu, R. The Impact of the Number of Layers of a Graphene Nanopore on DNA Translocation. *Soft Matter* **2013**, *9* (3), 960−966.
(16) Graf, M.; Lihter, M.; Thakur, M.; Georgiou, V.; Topolancik, J.; Ilic, B. R.; Liu, K.; Feng, J.; Astier, Y.; Radenovic, A. Fabrication and Practical Applications of Molybdenum Disulfide Nanopores. *Nat. Protoc.* **2019**, *14* (4), 1130−1168.
(17) Graf, M. *2D Nanopores: Fabrication, Energy Harvesting and Field-Effect Sensing.* **2019**, 231.
(18) Puster, M.; Balan, A.; Rodríguez-Manzo, J. A.; Danda, G.; Ahn, J. H.; Parkin, W.; Drndic, M. Cross-Talk between Ionic and Nanoribbon Current Signals in Graphene Nanoribbon-Nanopore Sensors for Single-Molecule Detection. *Small* **2015**, *11* (47), 6309−6316.
(19) Xie, P.; Xiong, Q.; Fang, Y.; Qing, Q.; Lieber, C. M. Local Electrical Potential Detection of DNA by Nanowire-Nanopore Sensors. *Nat. Nanotechnol.* **2012**, *7* (2), 119−125.
(20) de Souza, F. A. L.; Amorim, R. G.; Scopel, W. L.; Scheicher, R. H. Controlled Current Confinement in Interfaced 2D Nanosensor for Electrical Identification of DNA. *Phys. Chem. Chem. Phys.* **2019**, *21* (45), 24884−24890.
(21) Nelson, T.; Zhang, B.; Prezhdo, O. V. Detection of Nucleic Acids with Graphene Nanopores: Ab Initio Characterization of a Novel Sequencing Device. *Nano Lett.* **2010**, *10* (9), 3237−3242.
(22) Ouyang, F.-P.; Peng, S.-L.; Zhang, H.; Weng, L.-B.; Xu, H. A Biosensor Based on Graphene Nanoribbon with Nanopores: A First-Principles Devices-Design. *Chin. Phys. B* **2011**, *20* (5), 058504.
(23) Parkin, W. M.; Drndić, M. Signal and Noise in FET-Nanopore Devices. *ACS Sensors* **2018**, *3* (2), 313−319.
(24) Augustus, M., IV On the Influence of Temperature on the Electric Conducting-Power of Alloys. *Philos. Trans. R. Soc. London* **1864**, *154*, 167−200.
(25) Radisavljevic, B.; Radenovic, A.; Brivio, J.; Giacometti, V.; Kis, A. Single-Layer MoS2 Transistors. *Nat. Nanotechnol.* **2011**, *6* (3), 147−150.
(26) Late, D. J.; Liu, B.; Matte, H. S. S. R.; Dravid, V. P.; Rao, C. N. R. Hysteresis in Single-Layer MoS 2 Field Effect Transistors. *ACS Nano* **2012**, *6* (6), 5635−5641.
(27) Wang, J.; Yao, Q.; Huang, C.-W.; Zou, X.; Liao, L.; Chen, S.; Fan, Z.; Zhang, K.; Wu, W.; Xiao, X.; Jiang, C.; Wu, W.-W. High Mobility MoS 2 Transistor with Low Schottky Barrier Contact by Using Atomic Thick H-BN as a Tunneling Layer. *Adv. Mater.* **2016**, *28* (37), 8302−8308.
(28) Novoselov, K. S.; Jiang, D.; Schedin, F.; Booth, T. J.; Khotkevich, V. V.; Morozov, S. V.; Geim, A. K. Two-Dimensional Atomic Crystals. *Proc. Natl. Acad. Sci. U. S. A.* **2005**, *102* (30), 10451−10453.
(29) Baugher, B. W. H.; Churchill, H. O. H.; Yang, Y.; Jarillo-Herrero, P. Intrinsic Electronic Transport Properties of High-Quality Monolayer and Bilayer MoS 2. *Nano Lett.* **2013**, *13* (9), 4212−4216.
(30) Lu, Z.; Serrao, C.; Khan, A. I.; Clarkson, J. D.; Wong, J. C.; Ramesh, R.; Salahuddin, S. Electrically Induced, Non-Volatile, Metal Insulator Transition in a Ferroelectric-Controlled MoS 2 Transistor. *Appl. Phys. Lett.* **2018**, *112* (4), 043107.
(31) Parkin, W. M.; Balan, A.; Liang, L.; Das, P. M.; Lamparski, M.; Naylor, C. H.; Rodríguez-Manzo, J. A.; Johnson, A. T. C.; Meunier, V.; Drndić, M. Raman Shifts in Electron-Irradiated Monolayer MoS 2. *ACS Nano* **2016**, *10* (4), 4134−4142.
(32) Masih Das, P.; Drndić, M. In Situ 2D MoS 2 Field-Effect Transistors with an Electron Beam Gate. *ACS Nano* **2020**, *14* (6), 7389−7397.
(33) Chen, K.; Bell, N. A. W.; Kong, J.; Tian, Y.; Keyser, U. F. Direction- and Salt-Dependent Ionic Current Signatures for DNA Sensing with Asymmetric Nanopores. *Biophys. J.* **2017**, *112* (4), 674−682.
(34) Qiu, H.; Girdhar, A.; Schulten, K.; Leburton, J. P. Electrically Tunable Quenching of DNA Fluctuations in Biased Solid-State Nanopores. *ACS Nano* **2016**, *10* (4), 4482−4488.
(35) Humphrey, W.; Dalke, A.; Schulten, K. VMD: Visual Molecular Dynamics. *J. Mol. Graphics* **1996**, *14* (1), 33−38.
(36) Stewart, J. A.; Spearot, D. E. Atomistic Simulations of Nanoindentation on the Basal Plane of Crystalline Molybdenum Disulfide (MoS 2). *Modell. Simul. Mater. Sci. Eng.* **2013**, *21* (4), 045003.
(37) van Dijk, M.; Bonvin, A. M. J. J. 3D-DART: A DNA Structure Modelling Server. *Nucleic Acids Res.* **2009**, *37*, W235−W239.
(38) Foloppe, N.; MacKerell, A. D., Jr All-Atom Empirical Force Field for Nucleic Acids: I. Parameter Optimization Based on Small Molecule and Condensed Phase Macromolecular Target Data. *J. Comput. Chem.* **2000**, *21* (2), 86−104.
(39) Elrod-Erickson, M.; Rould, M. A.; Nekludova, L.; Pabo, C. O. Zif268 Protein-DNA Complex Refined at 1.6å: A Model System for Understanding Zinc Finger-DNA Interactions. *Structure* **1996**, *4* (10), 1171−1180.
(40) Mark, P.; Nilsson, L. Structure and Dynamics of the TIP3P, SPC, and SPC/E Water Models at 298 K. *J. Phys. Chem. A* **2001**, *105* (43), 9954−9960.
(41) Yoo, J.; Aksimentiev, A. Improved Parametrization of Li + , Na + , K + , and Mg 2+ Ions for All-Atom Molecular Dynamics Simulations of Nucleic Acid Systems. *J. Phys. Chem. Lett.* **2012**, *3* (1), 45−50.
(42) Girdhar, A.; Sathe, C.; Schulten, K.; Leburton, J.-P. Graphene Quantum Point Contact Transistor for DNA Sensing. *Proc. Natl. Acad. Sci. U. S. A.* **2013**, *110* (42), 16748−16753.
(43) Phillips, J. C.; Braun, R.; Wang, W.; Gumbart, J.; Tajkhorshid, E.; Villa, E.; Chipot, C.; Skeel, R. D.; Kalé, L.; Schulten, K. Scalable Molecular Dynamics with NAMD. *J. Comput. Chem.* **2005**, *26* (16), 1781−1802.
(44) Essmann, U.; Perera, L.; Berkowitz, M. L.; Darden, T.; Lee, H.; Pedersen, L. G. A Smooth Particle Mesh Ewald Method. *J. Chem. Phys.* **1995**, *103* (19), 8577−8593.

https://dx.doi.org/10.1021/acsnano.0c08382
ACS Nano 2020, 14, 16131−16139

(45) Qiu, H.; Sarathy, A.; Schulten, K.; Leburton, J.-P. Detection and Mapping of DNA Methylation with 2D Material Nanopores. *npj 2D Mater. Appl.* **2017**, *1* (1), 3.
(46) Tabatabaei, S. K.; Wang, B.; Athreya, N. B. M.; Enghiad, B.; Hernandez, A. G.; Fields, C. J.; Leburton, J.-P.; Soloveichik, D.; Zhao, H.; Milenkovic, O. DNA Punch Cards for Storing Data on Native DNA Sequences via Enzymatic Nicking. *Nat. Commun.* **2020**, *11* (1), 1742.
(47) Xiong, M.; Graf, M.; Athreya, N.; Radenovic, A.; Leburton, J.-P. Microscopic Transport Analysis of Single Molecule Detection in MoS_2 Nanopore Membranes. *arXiv.org*, 2020, 2004.10695. http://arxiv.org/abs/2004.10695.

https://dx.doi.org/10.1021/acsnano.0c08382
ACS Nano 2020, 14, 16131−16139